C. R. Geoscience 344 (2012) 67–76

Contents lists available at SciVerse ScienceDirect

Comptes Rendus Geoscience

www.sciencedirect.com

Petrology, geochemistry

Diamond precipitation from ascending reduced fluids in the Kaapvaal lithosphere: Thermodynamic constraints

Précipitation de diamant lors de l'ascension de fluides réduits au sein de la lithosphère du Kaapvaal : contraintes thermodynamiques

Jan Marten Huizenga [a,*], Alexandra Crossingham [b], Fanus Viljoen [b]

[a] *School of Environmental Sciences and Development, Department of Geology, North-West University, Private Bag X6001, 2520 Potchefstroom, South Africa*
[b] *Department of Geology, University of Johannesburg, PO Box 524, Auckland Park, 2006 Johannesburg, South Africa*

ARTICLE INFO

Article history:
Received 29 August 2011
Accepted after revision 6 January 2012
Available online 3 March 2012

Presented by Johan Zdenek

Keywords:
Diamond
Kaapvaal lithosphere
C-O-H fluid
Thermodynamic modelling
Redox melting

ABSTRACT

Previous research has shown that the Kaapvaal lithospheric mantle is generally reduced and characterised by a decreasing redox state with increasing depth. As a consequence, C-O-H fluids in the Kaapvaal lithospheric mantle are dominated by H_2O, CH_4, and C_2H_6. Thermodynamic calculations demonstrate that diamond precipitation from such a fluid during ascend is possible as it is exposed to a more oxidised environment and both CH_4 and C_2H_6 are oxidised. However, the calculations also demonstrate that the diamond precipitation potential from such a fluid decreases when: (1) the mantle is either more reduced or oxidised compared to the Kaapvaal mantle, or (2) the change in temperature with pressure is smaller compared to that of the Kaapvaal mantle. Therefore, the presence of reduced mantle fluid species and a generally decreasing oxygen fugacity with increasing depth do not necessarily warrant diamond precipitation from a rising reduced fluid.

Mots clés :
Diamant
Lithosphère Kaapvaal
Fluide C-O-H
Modélisation thermodynamique
Fusion redox

RÉSUMÉ

Des travaux précédents ont montré que le manteau lithosphérique du Kaapvaal est généralement réduit, caractérisé par un état redox décroissant à profondeur croissante. En conséquence, les fluides C-O-H dans le manteau lithosphérique du Kaapvaal sont dominés par H_2O, CH_4, et C_2H_6. Des calculs thermodynamiques montrent que le potentiel de précipitation de diamant à partir d'un tel fluide lors de son ascension est possible, lorsqu'il est exposé à un environnement plus oxydant et que CH_4 et C_2H_6 sont tous deux oxydés. Toutefois, ces calculs démontrent également que la capacité de dépôt de diamant à partir d'un tel fluide diminue lorsque : (1) le manteau est, soit plus oxydé, soit plus réduit que le manteau du Kaapvaal et (2) la variation de température en fonction de la pression est plus faible que celle du manteau du Kaapvaal. En conséquence, la présence d'une espèce réduite dans le fluide mantélique et une fugacité d'oxygène généralement décroissante avec la pression n'impliquent pas nécessairement le dépôt de diamant lors de l'ascension d'un fluide réduit.

1. Introduction

Multiple lines of evidence reviewed by Cartigny (2005) and Cartigny et al. (2004) show that diamond formation in the mantle is associated with carbon-bearing fluids.

* Corresponding author.
E-mail address: jan.huizenga@nwu.ac.za (J.M. Huizenga).

1631-0713/$ – see front matter
doi:10.1016/j.crte.2012.01.001

Oxygen fugacity (f_{O_2}) estimates of the subcratonic lithosphere of the Kaapvaal (e.g., Woodland and Koch, 2003) and Slave (McCammon and Kopylova, 2004) Cratons show that, generally, f_{O_2} decreases with increasing depth relative to the Fayalite-Magnetite-Quartz (FMQ) oxygen buffer, e.g. $\log_{10} f_{O_2}$ is ~FMQ − 1 at ~100 km depth ~FMQ − 4 at a depth of ~220 km for the Kaapvaal Craton (e.g., Woodland and Koch, 2003). In such an environment, diamond may precipitate by reduction of a CO_2-rich fluid/melt that reacts with the reduced host rocks (e.g., Haggerty, 1999) in the subcontinental lithosphere. Alternatively, which is the topic of this study, diamond may also precipitate by oxidation of reduced mantle fluid species including CH_4 (Deines, 1980) and C_2H_6 as it rises (Taylor and Green, 1988, 1989).

The diamond precipitation reactions including $CH_4 + O_2 \rightarrow C + 2H_2O$ and $C_2H_6 + 1½O_2 \rightarrow 2C + 3H_2O$ result in an increase of the H_2O-activity, and subsequent (local) melting of the surrounding peridotitic mantle. This concept was introduced by Taylor and Green (1988, 1989) and referred to as redox melting, which is considered to be an important process in the cratonic mantle lithosphere (Foley, 2011). The redox melting proposition has gained significant support, based on the fact, as mentioned previously, that reduced fluid species are likely to exist in a mantle fluid, combined with a suitable f_{O_2} − depth profile (e.g. Galimov, 1991; Haggerty, 1999; Kadik, 2006; Stachel and Harris, 2009; Woodland and Koch, 2003). In addition, the chemistry of mineral inclusions in diamond (Jacob et al., 2004; Malkovets et al., 2007; Stachel and Harris, 1997) and stable isotope data of carbon and nitrogen (Thomassot et al., 2007) indicate that diamond precipitation from CH_4 is a distinct possibility.

The purpose of this study is, by using thermodynamic calculations, to determine: (1) the diamond precipitation potential from a reduced rising C-O-H fluid in the Kaapvaal cratonic mantle (KM), and (2) the influence of changing *P*, *T*, and f_{O_2} conditions on this process. Our aim is thus to test whether diamond precipitation, by means of redox melting, is feasible or not. So far, no quantitative study has been done before on mantle fluid oxidation and the associated diamond precipitation as a function of *P*, *T*, and f_{O_2}. The recently published themodynamic model for C-O-H fluids at mantle conditions (Zhang and Duan, 2009, 2010) and the existence of high-quality $P - T - f_{O_2}$ data for the KM have created an ideal opportunity to perform this study.

2. Fluid composition of the Kaapvaal cratonic mantle (KM)

2.1. P, T, and f_{O_2} data

As will be discussed in the section below, carbon-saturated C-O-H fluid compositions can be calculated if *P*, *T*, and f_{O_2} are known. Here, we used KM *P*, *T*, and f_{O_2} data obtained from garnet-olivine-clinopyroxene-orthopyroxene assemblages in non-metasomatised lherzolitic and harzburgitic xenoliths from different kimberlite localities in South Africa (Bultfontein, Finsch, Frank Smith, Jagersfontein, Kimberley, Monastery, Wesselton) and Lesotho (Letseng, Liqhobong, Matsoku) (Lazarov et al., 2009; McCammon et al., 2001; Woodland and Koch, 2003). For consistency, we only used *P*, *T*, and f_{O_2} data that were calculated from the Al-in orthopyroxene barometer, the two-pyroxene thermometer (Brey and Köhler, 1990), and the Fe^{2+}-Fe^{3+} redox reaction involving garnet, olivine and orthopyroxene (Gudmundsson and Wood, 1995; Luth et al., 1990), respectively. Only data in which Fe^{3+} in garnet was determined by Mössbauer spectroscopy were used. All f_{O_2} values are reported relative to FMQ, which is calculated as follows:

$$\log_{10} f_{O_2}^{\mathrm{FMQ}} = 82.75 + 0.00484/T\,(\mathrm{K}) - 30681T - 24.45\log_{10}T + 94P\ (\mathrm{kbar})/T - 0.002P$$

(Ballhaus et al., 1991; O'Neill, 1987). In order to calculate the compositional changes of a rising C-O-H fluid, the variation of both *T* and f_{O_2} with *P* are needed. Therefore, correlations between *P* and *T*, and *P* and f_{O_2} were determined, which can be expressed by the following exponential best fit equations: P (kbar) = 11.455 exp [0.0012 T (°C)] (Fig. 1A) and P (kbar) = 20.310 exp [−0.265 ΔFMQ] (Fig. 1B), in which ΔFMQ denotes $\log_{10} f_{O_2} - \log_{10} f_{O_2}^{\mathrm{FMQ}}$. In both cases, maximum coefficients of determination (R^2) were obtained for exponential correlations. The *P*-*T* correlation is excellent ($R^2 = 0.90$) and the best fit curve overlaps largely with the 43 mW/m^{-2} surface heat flow geotherm (Pollack and Chapman, 1977). The $P - f_{O_2}$ correlation ($R^2 = 0.64$) is reasonable. The $P - f_{O_2}$ best fit curve is almost perfectly parallel to the $P - f_{O_2}$ curves determined for isochemical systems (garnet $Fe^{3+}/\Sigma Fe = 0.055$, 0.10, see Fig. 1B) evolving along the 43 mW/m^{-2} geotherm (Creighton et al., 2009). Also, the $Fe^{3+}/\Sigma Fe$ values of the data are in good agreement with the calculated $P - f_{O_2}$ curves for isochemical systems (Fig. 1B). We have accommodated the scatter of the f_{O_2} data in our calculations (section 3.2).

2.2. C-O-H fluid composition calculations

A carbon-saturated (i.e., diamond or graphite present) C-O-H fluid generally comprises H_2O, CO_2, and CH_4 as the most dominant fluid species (e.g., French, 1966; Ohmoto and Kerrick, 1977). For such a system, the carbon activity in the fluid phase (a_c^{fluid}) is 1 and becomes invariant if f_{O_2} is known. Due to the reduced nature and relatively high *P* of KM, additional fluid species such as H_2 and C_2H_6 may also be present in significant quantities. The Gibbs energy minimisation method as proposed by Zhang and Duan (2009, 2010) is an appropriate thermodynamic model available for the calculation of the fluid composition at KM $P - T - f_{O_2}$ conditions. Here, the fluid composition is calculated by establishing the minimum Gibb's energy for the system using an equation of state that is valid for all relevant fluid species at mantle *P*-*T* conditions. All calculations were carried out using the Excel spreadsheet GFluid (Zhang and Duan, 2010). The details of the calculations and the equation of state used are given in Zhang and Duan (2009, 2010).

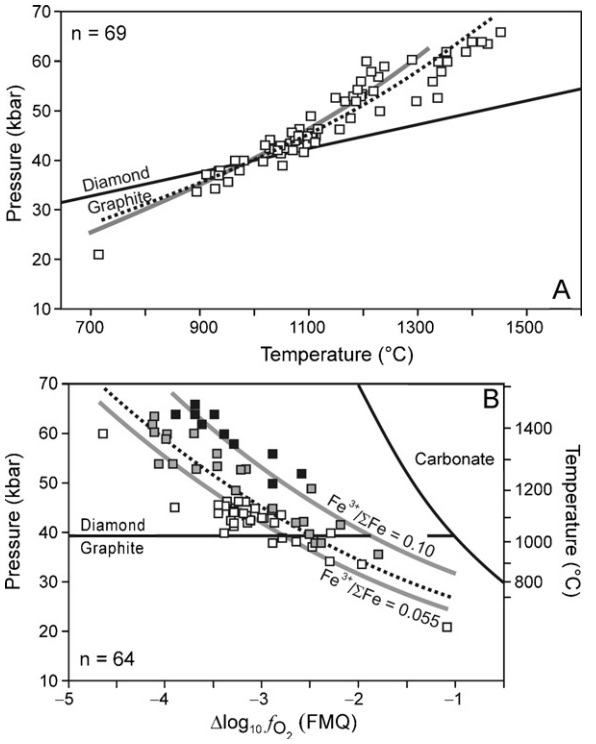

Fig. 1. (A) Xenolith-based *P-T* data for the Kaapvaal mantle (KM) (Lazarov et al., 2009; McCammon et al., 2001; Woodland and Koch, 2003). The best fit line for the *P-T* data (dotted line) overlaps almost perfectly with that of the 43 mW/m^{-2} surface heat flow geotherm (grey line, after Pollack and Chapman, 1977) and is given by the equation: P (kbar) = 11.455 exp [0.0012 T (°C)]. (B) $P - f_{O_2}$ data for KM (Lazarov et al., 2009; McCammon et al., 2001; Woodland and Koch, 2003). Black squares: samples with $Fe^{3+}/\Sigma Fe > 0.10$; grey squares: samples of which $0.055 \leq Fe^{3+}/\Sigma Fe \leq 0.10$; white squares: samples with $Fe^{3+}/\Sigma Fe < 0.055$. The best fit line for the $P - f_{O_2}$ data is given by the equation P (kbar) = 20.310 exp [−0.265 ΔFMQ]. Grey lines: $P - f_{O_2}$ relationship calculated for isochemical systems of which garnet $Fe^{3+}/\Sigma Fe = 0.10$ and 0.055 for the 43 mW/m^{-2} geotherm (grey lines) (Creighton et al., 2009). The carbonate stability field calculated from the enstatite-magnesite-olivine-graphite/diamond buffer (calculated for the best fit *P-T* curve) is indicated (Stagno and Frost, 2010). For both (A) and (B) the diamond-graphite boundary is calculated using GFluid (Zhang and Duan, 2010) from thermodynamic data by Fried and Howard (2000).

Fig. 1. (A) Conditions P-T estimées d'après des xénolithes du manteau du Kaapvaal (Lazarov et al., 2009 ; McCammon et al., 2001 ; Woodland and Koch, 2003). La meilleure ligne de régression pour ces données P-T (pointillés) suit à peu près parfaitement le géotherme correspondant à un flux de chaleur en surface de 43 mW/m^{-2} (ligne grise, d'après Pollack and Chapman, 1977), d'équation : P (kbar) = 11,455 exp [0,0012 T (°C)]. (B) Données $P - f_{O_2}$ pour Kaapvaal mantle (KM) (Lazarov et al., 2009 ; McCammon et al., 2001 ; Woodland and Koch, 2003). Carrés noirs : échantillons dont $Fe^{3+}/\Sigma Fe > 0,10$; carrés gris : échantillons pour lesquels $0,055 \leq Fe^{3+}/\Sigma Fe \leq 0,10$; carrés vides : échantillons dont $Fe^{3+}/\Sigma Fe <$ 0,055. La meilleure ligne de régression pour les données $P - f_{O_2}$ est fournie par l'équation P (kbar) = 20,330 exp [-0,265 FMQ]. Lignes grises : relation $P - f_{O_2}$ calculée pour les systèmes isochimiques dont le grenat $Fe^{3+}/\Sigma Fe$ = - 0,10 et 0,055 pour le géotherme 43 mW/m^{-2} (lignes grises) (Creighton et al., 2009). Le champ de stabilité du carbonate, calculé à partir du tampon enstatite-magnésite-olivine-graphite/diamant (calculé pour la meilleure courbe de régression *P-T*) est indiqué (Stagno et Frost, 2010). Pour A et B, la limite diamant/graphite est calculée en utilisant Gfluid (Zhang et Duan, 2010) à partir des données thermodynamiques et Fried et Howard (2000).

The GFluid model has been compared with experimental results within the *P-T* range of 5–30 kbar and 1000–1500 °C, respectively, showing differences generally within ±5% (Zhang and Duan, 2009). At $P > 30$ kbar, however, experimental data (Sokol et al., 2009) show significant quantities of C_2H_6 and H_2, at the expense of CH_4, in contrast to the calculated fluid compositions (Sokol et al., 2009). Both C_2H_6 and H_2 are the products of the partial dissociation of CH_4 (e.g., Scott et al., 2004; Spanu et al., 2011). The GFluid model appears to underestimate the effect of partial dissociation of CH_4 (Sokol et al., 2009). However, a molecular dynamics study performed by Spanu et al. (2011) appears to solve this contradiction. This study shows that the actual dissociation of CH_4 requires transition metals (in particular noble metals such as Ir) and that CH_4 occurs in metastable conditions if

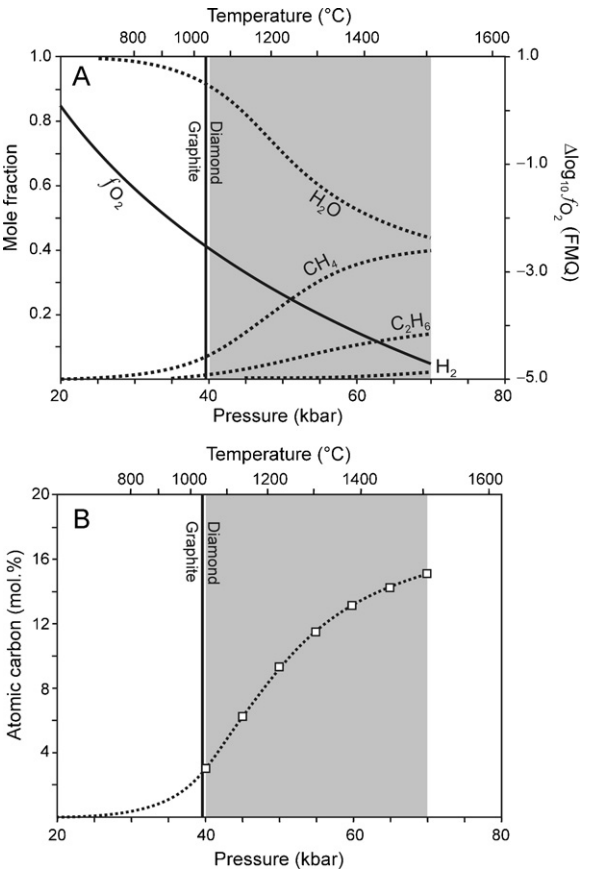

Fig. 2. (A) Carbon-saturated fluid compositions calculated as a function of *P* for Kaapvaal mantle (KM), using the best fit equations between *P-T* and $P - f_{O_2}$ (Fig. 1) illustrating that the main fluid species at *P* between 40 and 70 kbar (grey area) are H_2O, CH_4 and C_2H_6. (B) Variation of the fluid atomic carbon content (dotted line) for the carbon-saturated fluid compositions calculated as a function of *P* for KM (see A). Squares: fluid atomic carbon content at 70 to 40 kbar (5 kbar interval).

Fig. 2. (A) Compositions de fluides saturés en carbone, calculées en fonction de P pour Kaapvaal mantle (KM), en utilisant les meilleures courbes de régression entre *P-T* and $P - f_{O_2}$ (Fig. 1), illustrant le fait que les espèces les plus importantes pour *P* entre 40 and 70 kbar (surface grise) sont H_2O, CH_4 and C_2H_6. (B) Variation de la teneur en carbone atomique du fluide (ligne pointillée) pour des compositions saturées en carbone, calculées en fonction de P pour KM (voir A). Carrés : teneur du fluide en carbone atomique de 70 à 40 kbar (intervalles de 5 kbar).

these metals are absent. As mantle metal saturation is only to be expected at $P > \sim 80$ kbar (Frost and McCammon, 2008, Rohrbach et al., 2011), CH_4 is expected to exist in a metastable condition (Spanu et al., 2011) at $P < \sim 80$ kbar. Consequently, the GFluid thermodynamic model can be used for the purpose of this study if $P < 80$ kbar.

Using the correlations between P and T (Fig. 1A), and P and f_{O_2} (Fig. 1B), the composition of a C-O-H fluid in KM can be calculated (Fig. 2A) as a function of pressure. The calculation results are summarised as follows (Fig. 2A): (1) An ambient C-O-H fluid in KM will be dominated by H_2O, CH_4 and C_2H_6 whereas CO_2 will be absent; (2) The concentrations of CH_4, C_2H_6 and H_2 increase with depth at the expense of H_2O; (3) The atomic carbon content of the fluid phase increases with pressure (Fig. 2B). (4) Not only CH_4, but also C_2H_6 is a potential fluid species from which diamond can precipitate by oxidation. These results are in good agreement with those from other studies (e.g. Kadik, 2006; Saxena, 1989; Simakov, 1998; Wood et al., 1990; Zhang and Duan, 2009).

3. Thermodynamic modelling of a rising reduced fluid through Kaapvaal cratonic mantle (KM)

3.1. Kaapvaal cratonic mantle (KM) $P-T-f_{O_2}$ conditions

The thermodynamic factors involved in the precipitation of diamond from an upwards percolating reduced fluid in the subcratonic lithosphere, include changes in ambient pressure and temperature, as well as changes in f_{O_2} of the fluid phase (which is controlled by f_{O_2} of the surrounding mantle lithosphere with which it equilibrates). Isobaric-isothermal C-O-H ternary diagrams are appropriate for visualising and assessing the process of diamond crystallisation from such an upward moving mantle fluid.

Fig. 3A shows a C-O-H ternary diagram that is calculated at an arbitrarily chosen fixed P and T of 50 kbar and 1227 °C, respectively, that plots on the best fit P-T curve (Fig. 1A). The C-O-H ternary diagram is characterised by a fluid-only region (white area in Fig. 3A) and a field of fluid + diamond (grey area in Fig. 3A). These are separated from each other by the carbon saturation surface (black line in Fig. 3A). The carbon saturation surface represents the variation of carbon-saturated ($a_c^{fluid} = 1$) C-O-H fluid compositions as a function of f_{O_2} (Fig. 3B, C). Fluids situated on the carbon saturation are in dynamic equilibrium with diamond, i.e. there is no net consumption or production of diamond. However, any changes of P, T and/or f_{O_2} disturbs this equilibrium and may result in either the crystallisation of diamond from the fluid or in the resorption of diamond by the fluid. Fluid compositions that are situated in the grey field (Fig. 3A) are supersaturated in carbon. Studies for the graphite-C-O-H fluid system have shown that in such a case the graphite that precipitates is poorly crystalline (Ziegenbein and Johannes, 1989). Therefore, it is expected that, in the diamond stability field, carbon supersaturated fluids will probably result in the precipitation of poor quality diamond such as polycrystalline aggregates (Bureau et al., 2012; Sunagawa,

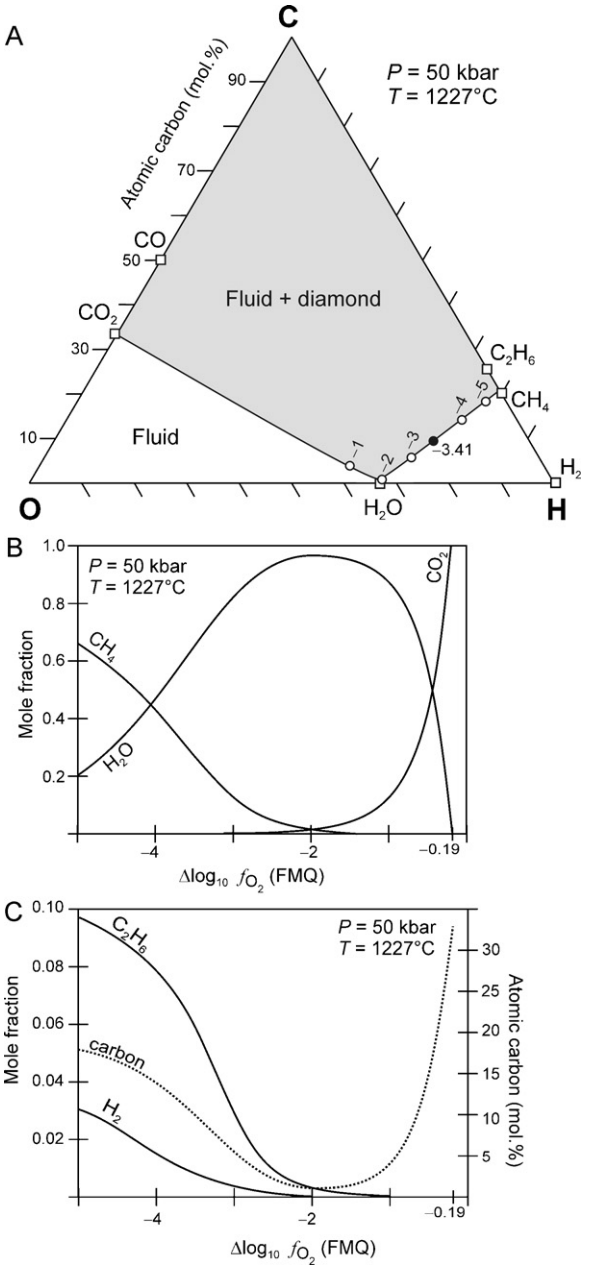

Fig. 3. (A) C-O-H ternary diagram constructed at 50 kbar and 1227 °C. Solid line: carbon saturation surface, i.e. all fluid compositions in equilibrium with diamond are located on this surface. Open circles: $\log_{10} f_{O_2}$ values relative to FMQ. Black circle: carbon-saturated fluid composition for Kaapvaal mantle (KM) $\log_{10} f_{O_2}$ at 50 kbar and 1227 °C: FMQ − 3.41. See text for further explanation. (B) and (C) Variation of a C-O-H fluid composition and the fluid atomic carbon content along the carbon saturation surface (see A) as a function of f_{O_2} at 50 kbar and 1227 °C.

Fig. 3. (A) Diagramme ternaire C-O-H à 50 kbar et 1227 °C. Trait continu : surface de saturation en carbone, i.e. toutes les compositions de fluides en équilibre avec le diamant sont situées sur cette surface. Cercles vides : valeurs de $\log_{10} f_{O_2}$ relativement à FMQ. Cercle noir : composition du fluide saturé en carbone pour Kaapvaal mantle (KM) $\log_{10} f_{O_2}$ à 50 kbar et 1227 °C : FMQ − 3,41. Voir le texte pour plus d'explications. (B) et (C) Variation de la composition d'un fluide C-O-H et de la teneur en carbone atomique le long de la surface de saturation en carbone (voir A) en fonction de f_{O_2} à 50 kbar et 1227 °C.

1990). Carbon undersaturated fluids, on the other hand, are situated in the white field in Fig. 3A, and these fluids will have the ability to dissolve diamond if present.

For the specified *P-T* conditions, a C-O-H fluid is dominated by H_2O and CO_2 if it is relatively oxidised (i.e., $(\mathrm{FMQ} - 0.19 > \log_{10} f_{O_2} > \mathrm{FMQ} - 2)$ (Fig. 3B) whereas, when more reduced $(\log_{10} f_{O_2} < \mathrm{FMQ} - 2)$, it will comprise predominantly of H_2O and CH_4, and, to a lesser extent, also C_2H_6 and H_2 (Fig. 3B, C). The fluid is carbon undersaturated if $\log_{10} f_{O_2} > \mathrm{FMQ} - 0.19$, in which case diamond cannot coexist with the fluid.

The carbon saturation surface in a C-O-H ternary diagram will move downwards towards the O-H binary with isobaric cooling (i.e., increasing the diamond stability field) whereas it will move upwards towards the C apex with isothermal decompression (i.e., decreasing the diamond stability field). This is an important fact that must be emphasised; the diamond stability field in a diamond-C-O-H fluid system may either increase or decrease during cooling and decompression, depending on $\Delta T/\Delta P$ of the geotherm. If the diamond stability decreases, diamond precipitation from a rising C-O-H fluid

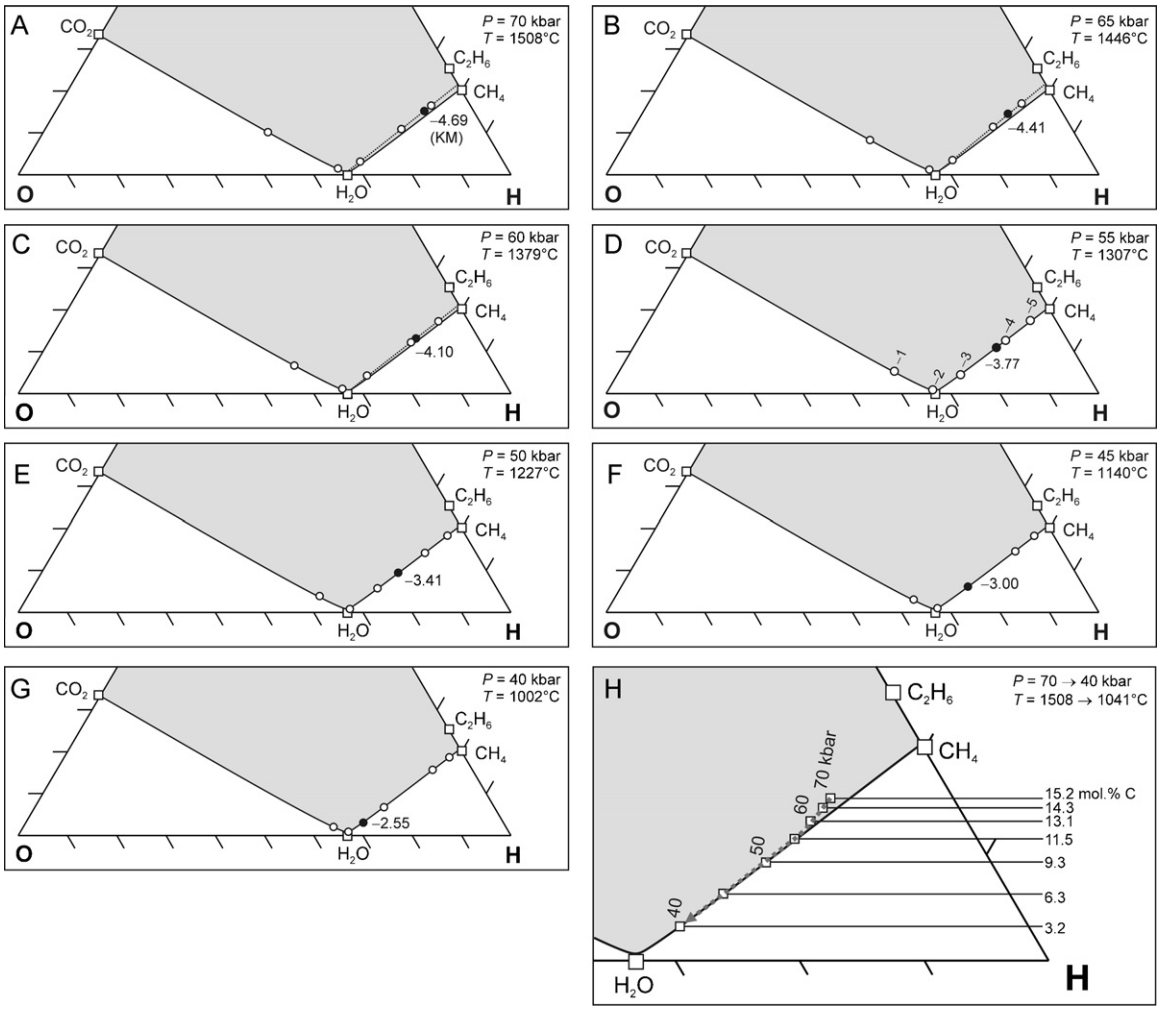

Fig. 4. (A–G) C-O-H ternary diagrams showing carbon saturation surfaces calculated for *P* = 70 to 40 kbar (5 kbar interval), and corresponding *T* calculated from the best fit *P-T* equation (Fig. 1A). The f_{O_2} of Kaapvaal mantle (KM) (black circles) are indicated at each pressure and calculated from the best fit $P - f_{O_2}$ equation (Fig. 1B). Open circles: $\log_{10} f_{O_2}$ values relative to FMQ as indicated in D. (H) Compilation of (A–G). The carbon saturation surfaces for 55, 50, 45, and 40 kbar, and their corresponding temperatures overlap completely. The 70, 65 and 60 kbar carbon saturation surfaces are situated slightly above the others (dotted lines). The compositional evolution of an upward migrating fluid in KM is shown by the grey dashed arrow. The decrease in the fluid atomic carbon content with decreasing pressure (15.2 mol.% at 70 kbar to 3.2 mol.% at 40 kbar) is caused by diamond precipitation. See text for further discussion.

Fig. 4. (A–G) Diagrammes ternaires C-O-H indiquant les surfaces de saturation en carbone, calculées pour *P* = 70 à 40 kbar (intervalles de 5 kbar), ainsi que T correspondant, calculé d'après les courbes de régression P-T (Fig. 1A). Les f_{O_2} de Kaapvaal mantle (KM) (cercles noirs) sont indiquées pour chaque pression et calculées en fonction de la courbe de régression de l'équation $P - f_{O_2}$ (Fig. 1B). Cercles blancs : valeurs de $\log_{10} f_{O_2}$ relativement à FMQ, ainsi qu'indiqué en D. (H) Compilation de (A–G). Les surfaces de saturation en carbone pour 55, 50, 45, and 40 kbar, et leurs températures correspondantes, se recouvrent complètement. Les surfaces de saturation en carbone pour 70, 65 and 60 kbar sont situées légèrement au-dessus des surfaces précédentes (lignes pointillées). L'évolution de la composition d'un fluide migrant vers le haut dans KM est indiquée par la flèche grise tiretée. La décroissance des teneurs en carbone atomique à pression décroissante (de 15,2 mol.% à 70 kbar à 3,2 mol.% à 40 kbar) est provoquée par la précipitation de diamant. Voir le texte pour une discussion plus détaillée.

would be impossible as the fluid becomes carbon undersaturated. Alternatively, the diamond stability field of a diamond-C-O-H fluid system may also increase during cooling and decompression, in which case the rising C-O-H fluid becomes carbon supersaturated. Therefore, in order to evaluate the possibility of diamond precipitation from a rising reduced fluid caused by oxidation, both $\Delta T/\Delta P$ and $\Delta f_{O_2}/\Delta P$ must be taken into consideration.

We considered a pressure interval of 70 to 40 kbar (5 kbar intervals) for the thermodynamic calculations, which is based on the total range of reported diamond crystallisation pressures (Phillips et al., 2004; Stachel and Harris, 2008). For each P we: (1) calculated the corresponding T and f_{O_2} from the best fit equations (Fig. 1), (2) determined the carbon saturation surface in a C-O-H ternary diagram at the specified P and T, and (3) determined the unique C-O-H fluid composition for the given $P-T-f_{O_2}$ conditions. The results of these calculations are shown in Fig. 4A–G and combined into one (Fig. 4H) for interpretative purposes.

The carbon saturation surfaces at 40, 45, 50, and 55 kbar are at the exact same position in a C-O-H ternary diagram, whereas at 60, 65 and 70 kbar the carbon saturation surface is positioned slightly above the others (Fig. 4H). This implies that a rising KM C-O-H fluid is carbon saturated or becomes slightly supersaturated. In other words, the KM geothermal conditions allow diamond precipitation from a rising C-O-H fluid as the condition of carbon saturation is met. Further, the fact that the fluid is only slightly carbon supersaturated implies that the diamonds that precipitate from such a fluid are likely to be highly crystalline (Ziegenbein and Johannes, 1989), i.e. typical of that utilised in the gem industry (single crystals or simple twins of good transparency) as opposed to industrial quality boart (Bureau et al., 2012; Sunagawa, 1990).

During migration over a depth interval corresponding to an ascent from 70 to 40 kbar pressure, the fluid H_2O concentration increases whereas the concentrations of CH_4 and C_2H_6 decrease (grey dashed arrow in Fig. 4H). Consequently, the atomic carbon content of the fluid phase decreases, which is due to the precipitation of diamond. This change in atomic carbon content can thus be used as an indication of the diamond precipitation potential of the fluid. The overall change in fluid atomic carbon content between 70 and 40 kbar is 12.0 mol.% (Fig. 4H). A comparison of the relative differences in fluid atomic carbon content for each 5 kbar interval (Fig. 2B, Fig. 4H) shows a gradual increase with decreasing P (Fig. 2B, Fig. 4H): from 0.9 mol.% (between 70 and 65 kbar) to 3.1 mol.% (between 45 and 40 kbar). This implies an increase of the diamond precipitation potential with decreasing P.

The reactions that are responsible for the change in the fluid composition can be deduced from the direction of the arrow in the C-O-H ternary diagram (cf. Fig. 4H and Fig. 5) and include the net oxidation reaction (direction 1 in Fig. 5):

$$CH_4 + O_2 \rightarrow C + 2H_2O \quad (1)$$

and (direction 2 in Fig. 5):

$$C_2H_6 + 1\mathbf{frac12;O_2} \rightarrow 2C + 3H_2O \quad (2)$$

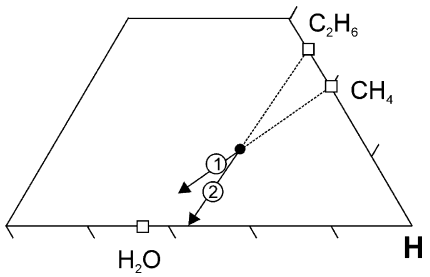

Fig. 5. C-O-H ternary diagram showing the expected compositional change (indicated with the arrows) for a H_2O-CH_4-C_2H_6 fluid as a result of the following net diamond precipitation reactions: 1, $CH_4 + O_2 \rightarrow 2H_2O + C$; 2, $C_2H_6 + 1½O_2 \rightarrow 3H_2O + 2C$.

Fig. 5. Diagramme ternaire C-O-H indiquant les variations de composition (indiquées par les flêches) d'un fluide H_2O-CH_4-C_2H_6 lors de la précipitation de diamant, d'après les réactions : 1, $CH_4 + O_2 \rightarrow 2H_2O + C$; 2, $C_2H_6 + 1½O_2 \rightarrow 3H_2O + 2C$.

Comparing Fig. 4H and Fig. 5 indicates that both reaction (1) and (2) take place at $P > 60$ kbar, whereas at $P < 60$ kbar reaction (1) dominates. The oxygen that is required for the reactions is extracted from the surrounding lithosphere, i.e. the lithosphere acts as an oxygen source. Alternatively, the reactions can also be written in an oxygen-absent manner:

$$CH_4 \rightarrow C + 2H_2 \quad (3)$$

$$C_2H_6 \rightarrow 2C + 3H_2 \quad (4)$$

in which case the surrounding lithosphere acts as a hydrogen reservoir. In presence of water, reactions (1) and (2) are thermodynamically equivalent to reactions (3) and (4), respectively (Eugster, 1959).

The calculation results can be compared with diamond crystallisation pressures, using Brey and Köhler's (1990) Al-in orthopyroxene barometer, based on non-touching garnet-orthopyroxene inclusion pairs in diamonds from the De Beers Pool kimberlites in Kimberley (Phillips et al., 2004) (Fig. 6). Some care should be taken with comparing the model calculations with the data by Phillips et al. (2004) (Fig. 6). First, Phillips et al. (2004) calculated temperatures with the garnet-orthopyroxene thermometer (Harley, 1984) and not the two-pyroxene thermometer (like all the other data used in this study) as clinopyroxene was absent. Second, the crystallisation pressures are slightly higher compared to the best fit geotherm (Fig. 6A). Lastly, a few of the Kimberley samples deviate from the best fit $P-f_{O_2}$ curve (Fig. 6B). However, despite these limitations, we feel that the comparison of our results with those of Phillips et al. (2004) will give some indication on whether diamond precipitation from a reduced fluid can be supported or should be rejected outright. The data by Phillips et al. (2004) show that more diamonds tend to crystallise as the pressure decreases (Fig. 6 C). This is in reasonable good agreement with the model calculations (Fig. 6 C).

3.2. Variable Kaapvaal cratonic mantle (KM) redox conditions

Although a reasonable good correlation was found between $P-f_{O_2}$, it is to be expected (as shown by the

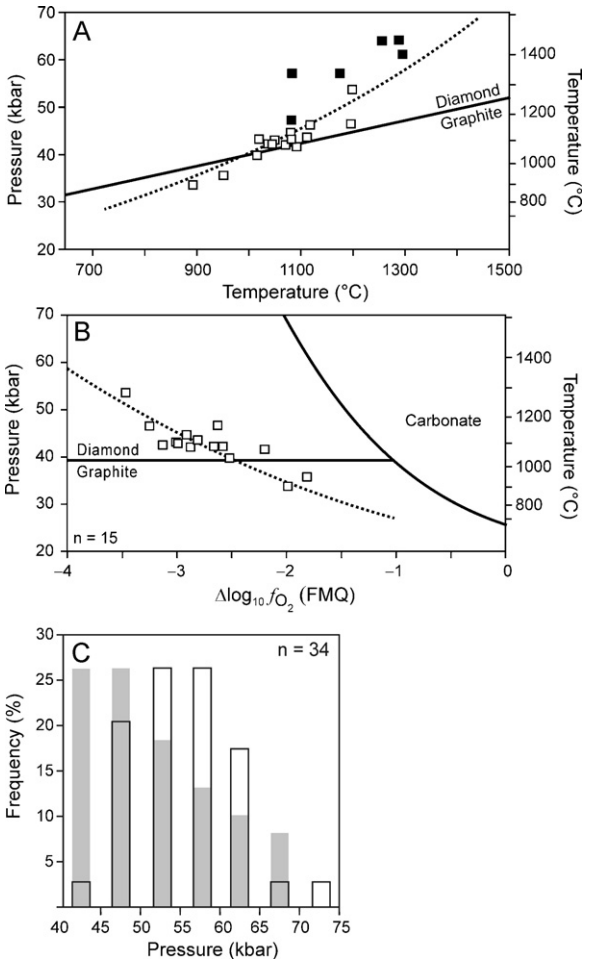

Fig. 6. (A) *P-T* data of Kimberley xenoliths (open squares) and Kimberley diamond inclusions (solid squares). Dotted line: best fit line obtained from xenolith data (Fig. 1A). (B) $P - f_{O_2}$ data of Kimberley xenoliths (open squares). Dotted line: best fit line obtained from xenolith data (Fig. 1B). (C) Histogram (black outlined bars) showing crystallisation pressure estimations of Kimberley diamonds (Phillips et al., 2004). The grey bars indicate the expected frequency of crystallisation pressures based on the calculation results (Fig. 4H). These results were converted into frequencies for different pressure intervals by normalising the differences in fluid atomic carbon content for each 5 kbar interval against the total change (from 70 to 40 kbar) of the fluid atomic carbon content.

Fig. 6. (A) Données P-T des xénolithes de Kimberley (carrés vides) et des inclusions dans les diamants de Kimberley (carrés pleins). Ligne pointillée : courbe de régression d'après les données des xénolithes (Fig. 1A). (B) Données $P - f_{O_2}$ des xénolithes de Kimberley (carrés vides). Ligne pointillée : courbe de régression à partir des données des xénolithes (Fig. 1B). (C) Histogramme (barres soulignées en noir) des pressions estimées de cristallisation des diamants de Kimberley (Phillips et al., 2004). Les barres grises indiquent les fréquences attendues des pressions lors de la cristallisation, d'après les résultats des calculs (Fig. 4H). Les fréquences pour les différents intervalles de pression ont été obtenues en normalisant les différences de teneur en carbone atomique du fluide par intervalle de 5 kbar par rapport à la variation totale entre 70 et 40 kbar.

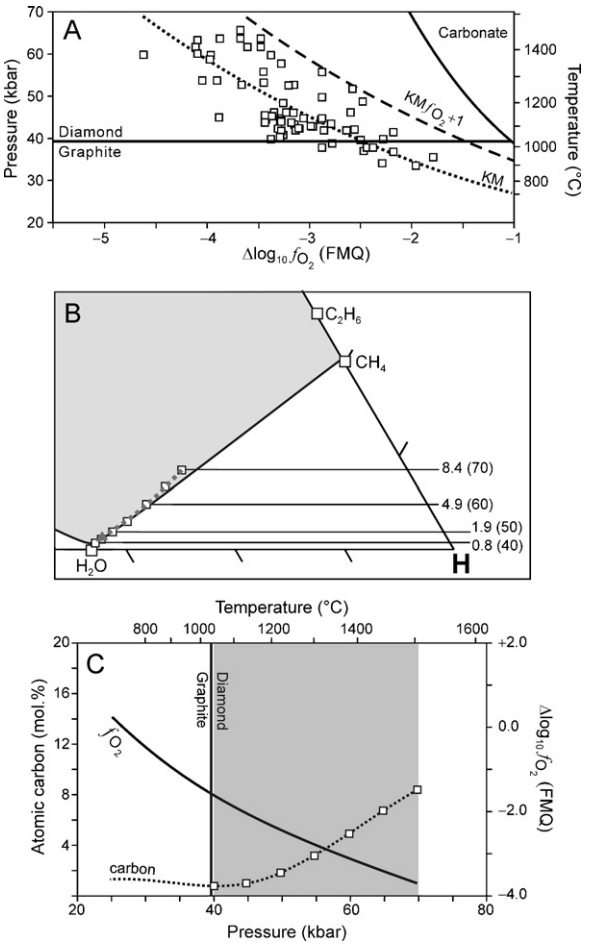

Fig. 7. (A) $P - f_{O_2}$ relationship (Kaapvaal mantle (KM) $f_{O_2} + 1$) used for modelling calculations (dashed line) of which the results are illustrated in (B) and (C). (B) C-O-H ternary diagram showing fluid compositions calculated for 70 to 40 kbar (5 kbar interval) and corresponding *T* calculated from the best fit *P-T* equation (Fig. 1A). Fluid atomic carbon content is indicated for 70–40 kbar (10 kbar interval). (C) Variation of f_{O_2} (solid line) and the fluid atomic carbon content (dotted line) as a function of pressure. Squares: fluid atomic carbon content at 70 to 40 kbar (5 kbar interval).

Fig. 7. (A) Relation $P - f_{O_2}$ (Kaapvaal mantle (KM) $f_{O_2} + 1$) utilisée pour la modélisation (ligne tiretée), dont les résultats sont donnés en (B) and (C). (B) Diagramme ternaire C-O-H indiquant les compositions calculées du fluide entre 70 et 40 kbar (intervalles de 5 kbar) et les *T* correspondantes, calculées d'après la courbe de régression de l'équation *P-T* (Fig. 1A). La teneur du fluide en carbone atomique est donnée pour 70-40 kbar (intervalles de 10 kbar). (C) Variation de f_{O_2} (ligne continue) et de la teneur en carbone atomique (ligne tiretée) en fonction de la pression. Carrés : teneur du fluide en carbone atomique de 70 à 40 kbar (intervalle de 5 kbar).

scatter of data points in Fig. 1B) that there are lateral f_{O_2} variations within KM (Luth, 1999). In order to evaluate the effect of varying redox conditions on the composition of an ascending C-O-H fluid and the crystallisation of diamond, we have performed calculations of C-O-H fluid compositions for two possible scenarios. In the first scenario, we assume that f_{O_2} of the surrounding mantle (over the entire depth interval of interest) is one $\log_{10}$ unit higher (i.e., more oxidised) than for KM (KM $f_{O_2} + 1$, Fig. 7). In the second scenario f_{O_2} is considered to be one $\log_{10}$ unit lower than KM (KM $f_{O_2} - 1$, Fig. 8). These two scenarios were chosen so that the entire scatter of the $P - f_{O_2}$ data points are accommodated for (Fig. 7A, Fig. 8A). The results of these two scenarios are compared to that of KM (Fig. 9).

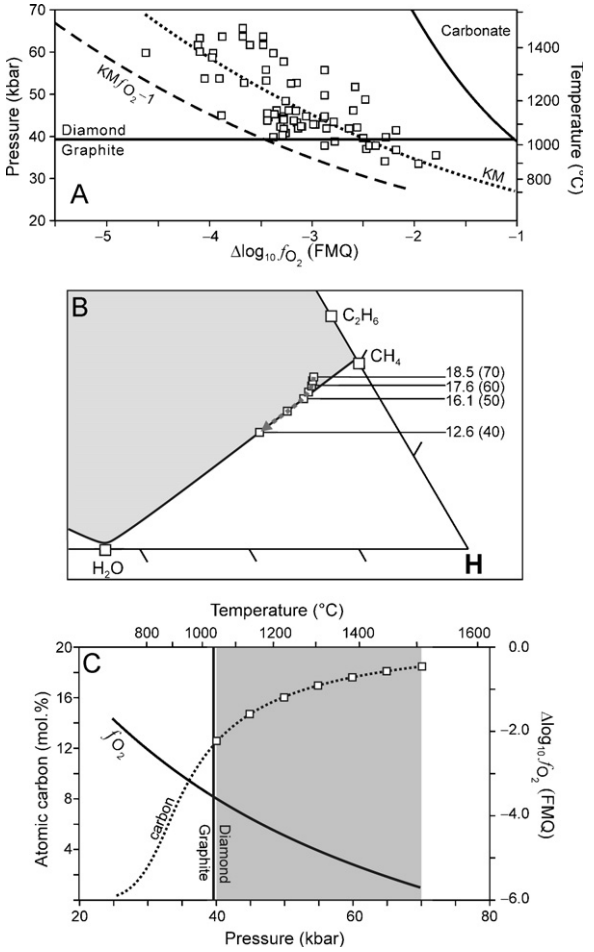

Fig. 8. (A) $P - f_{O_2}$ relationship (Kaapvaal mantle (KM) $f_{O_2} - 1$) used for modelling calculations (dashed line) of which the results are illustrated in (B) and (C). (B) C-O-H ternary diagram showing fluid compositions calculated for 70 to 40 kbar (5 kbar interval) and corresponding T calculated from the best fit P-T equation (Fig. 1A). Fluid atomic carbon content is indicated for 70-40 kbar (10 kbar interval). (C) Variation of f_{O_2} (solid line) and the fluid atomic carbon content (dotted line) as a function of pressure. Squares: fluid atomic carbon content at 70 to 40 kbar (5 kbar interval).

Fig. 8. (A) Relation $P - f_{O_2}$ (Kaapvaal mantle (KM) $f_{O_2} - 1$) utilisée pour la modélisation (ligne tiretée), dont les résultats sont donnés en (B) and (C). (B) Diagramme ternaire C-O-H indiquant les compositions de fluide calculées entre 70 et 40 kbar (intervalles de 5 kbar), ainsi que les T correspondantes, calculées d'après la courbe de régression de l'équation P-T (Fig. 1A). La teneur en carbone atomique du fluide est indiquée entre 70- et 40 kbar (intervalles de 10kbar). (C) Variation de f_{O_2} (ligne continue) et teneur en carbone atomique du fluide (ligne pointillée) en fonction de la pression. Carrés : teneur en carbone atomique du fluide entre 70 et 40 kbar (intervalles de 5 kbar).

For the oxidised scenario (KM $f_{O_2} + 1$, Fig. 7A), the fluid is generally H_2O rich (Fig. 7B). The dominant net reaction for diamond precipitation in this instance is the oxidation of CH_4 according to reaction (1) (cf. Fig. 5 and Fig. 7B). Compared to KM, this scenario favours diamond crystallisation at $P > 60$ kbar (Fig. 9). However, at $P < 60$ kbar, the diamond precipitation potential is significantly less compared to KM (Fig. 9).

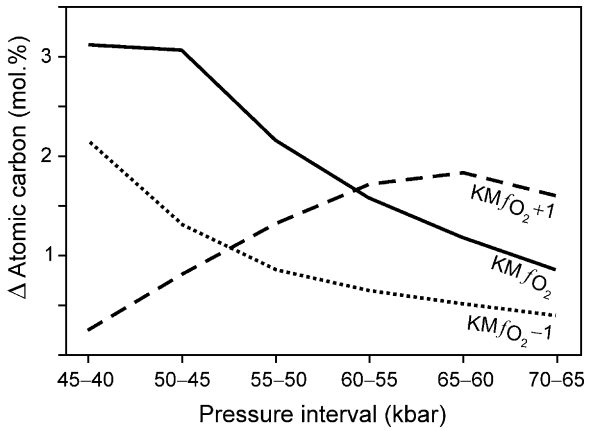

Fig. 9. Decrease in fluid atomic carbon content for different pressure intervals for the different scenarios as explained in the text. The decrease in atomic carbon content is the result of diamond precipitation and thus a reflection of the diamond precipitation potential.

Fig. 9. Décroissance de la teneur en carbone atomique du fluide pour les différents intervalles de pression, d'après les différents scénarios indiqués dans le texte. La décroissance des teneurs en carbone atomique résulte de la précipitation de diamant et indique donc le potentiel de formation de diamant.

A more reduced environment (KM $f_{O_2} - 1$, Fig. 8A) results in a systematic shift of the fluid compositional evolution towards a more CH_4-rich starting composition (Fig. 8B). The change in the fluid atomic carbon content between 70 and 40 kbar (Fig. 8B, C) is significantly less compared to that for KM (Fig. 9). The net diamond precipitation reaction at high P (70 to 60 kbar) is dominated by the oxidation of C_2H_6 according to reaction (2) (cf. Fig. 5 and Fig. 8B) whereas at $P < 60$ kbar kbar the oxidation of CH_4 (reaction (1)) is the dominant net diamond precipitation reaction (cf. Fig. 5 and Fig. 8B).

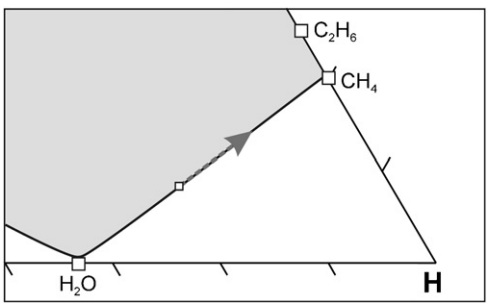

Fig. 10. Illustration of water removal from a carbon-saturated C-O-H fluid at isobaric-isothermal conditions. Removal of H_2O causes the fluid composition to move "back" along the carbon saturation surface to become more reduced relative to the host rock f_{O_2}. As a result, diamond crystallisation will occur by CH_4 oxidation. See text for further discussion.

Fig. 10. Illustration de l'effet de l'élimination de l'eau dans un fluide C-O-H saturé en carbone, à des conditions isobares-isothermes. L'élimination de l'eau fait se déplacer la composition du fluide "en arrière" le long de la surface de saturation en carbone, la rendant plus réduite par rapport à la f_{O_2} de la roche encaissante. Il en résulte une cristallisation de diamant par oxydation de CH_4. Voir le texte pour une discussion plus détaillée.

3.3. Effect of redox melting on diamond crystallisation

As mentioned previously, the increase of the H_2O activity results in partial melting of the mantle due to a decrease of the mantle solidus temperature (Foley, 2011; Taylor and Green, 1988, 1989). The H_2O will subsequently be removed from the fluid phase as it is concentrated in the melt phase (Foley, 2011). The elimination of H_2O from the fluid phase has an interesting effect on diamond crystallisation (Fig. 10). The removal of H_2O will "push" the fluid composition back along the carbon saturation surface to become more reduced relative to the host rock. As a result, diamond crystallisation will occur according to reaction (1) and/or (2) as the C-O-H fluid re-equilibrates towards the redox state of the host rock. Obviously, this process is dependent on the amount of H_2O that is removed, which is directly related to efficiency of the redox melting to physically remove H_2O from the fluid phase. It is important to note that the H_2O concentration in the fluid phase will increase again during diamond crystallisation, i.e. the entire process may repeat itself. The limiting factor to this repetition is the possibility to oxidise CH_4 and C_2H_6, which depends on the ability of the host rock to act either as an O_2 source or H_2 reservoir. In other words, the process will cease if the immediate surroundings of diamond crystallisation site cannot supply O_2 or absorb H_2.

4. Conclusions

The results of this study show that redox melting along with diamond precipitation is possible in the Kaapvaal lithospheric mantle because of its suitable $P-T-f_{O_2}$ environment. The calculations show that in such a case, crystallisation of diamond occurs of a carbon-saturated or slightly supersaturated C-O-H fluid, i.e. the diamonds that crystallise from such a fluid should be highly crystalline and of good quality. The removal of H_2O from the fluid phase by redox melting is an additional factor that would stimulate diamond crystallisation as it would result in a relative increase of CH_4 and C_2H_6 and thus fluid reduction. In this case, the redox difference between the fluid and the host rock is not caused by an ascending fluid into a more oxidised environment but by isobaric-isothermal reduction of the fluid due to H_2O removal. This effect, however, cannot be quantified as it depends on the exact amount of water that is removed.

The calculations demonstrate that diamond precipitation from a rising reduced fluid becomes less favourable when: (1) the environment is either more reduced or oxidised relative to the KM $P-f_{O_2}$ best fit curve, and (2) the cratonic lithosphere shows a cooler geotherm in comparison to the KM *P-T* best fit curve. In this case, the diamond stability field may actually decrease with decreasing *P* and *T*, i.e. the ascent of the reduced C-O-H fluid will render it to become carbon undersaturated and thus prohibit diamond precipitation.

Generally, it can be concluded that even if a reduced mantle fluid exists and f_{O_2} decreases with a depth, redox melting and the associated diamond precipitation may be insignificant or not possible. This might be in particular the case if lateral f_{O_2} variations disturb the general trend of decreasing f_{O_2} with increasing depth. Only high-quality $P-T-f_{O_2}$ data of the relevant region and thermodynamic calculations as done in this study can determine whether redox melting along with diamond crystallisation is a viable option.

Acknowledgements

This project was supported with funds from the DST Research Chair in Geometallurgy, administered by the National Research Foundation of South Africa (FV). Comments on a previous version of this manuscript by Katie Smart and Jeff Harris are highly appreciated. We would like to thank Pierre Cartigny and an anonymous reviewer for their detailed and constructive reviews.

References

Ballhaus, C., Berry, R.F., Green, D.H., 1991. High-pressure experimental calibration of the olivine-orthopyroxene-spinel oxygen barometer: implications for the oxidation state of the upper mantle. Contrib. Mineral. Petrol. 107, 27–40.

Brey, G.P., Köhler, T., 1990. Geothermobarometry in four-phase lherzolites II. New thermobarometers, and practical assessment of existing thermobarometers. J. Petrol. 31, 1353–1378.

Bureau, H., Langenhorst, F., Auzende, A.-L., Frost, D.J., Estève, I., Siebert, J., 2012. The growth of fibrous, cloudy and polycrystalline diamonds. Geochim. Cosmochim. Acta 77, 202–214.

Cartigny, P., 2005. Stable isotopes and the origin of diamonds. Elements 1, 79–84.

Cartigny, P., Stachel, T., Harris, J.W., Javoy, M., 2004. Constraining diamond metasomatic growth using C- and N-stable isotopes: examples from Namibia. Lithos 77, 359–373.

Creighton, S., Stachel, T., Matveev, S., Höfer, H., McCammon, C., Luth, R.W., 2009. Oxidation of Kaapvaal mantle driven by metasomatism. Contrib. Mineral. Petrol. 157, 491–504.

Deines, P., 1980. The carbon isotopic composition of diamonds: relationship to diamond shape, color, occurrence and vapour composition. Geochim. Cosmochim. Acta 44, 943–961.

Eugster, H.P., 1959. Oxidation and reduction in metamorphism. In: Ableson, P.H. (Ed.), Researches in Geochemistry. Wiley and Sons, pp. 397–426.

Foley, S.F., 2011. A reappraisal of redox melting in the Earth's mantle as a function of tectonic setting and time. J. Petrol. 52, 1363–1391.

French, B.M., 1966. Some geological implications of equilibrium between graphite and a C-O-H gas at high temperatures and pressures. Rev. Geophysics 4, 223–253.

Fried, L.E., Howard, W.M., 2000. Explicit Gibbs free energy equation of state applied to the carbon phase diagram. Phys. Rev. B: Condens. Matter 61, 8734–8743.

Frost, D.J., McCammon, C.A., 2008. The redox state of the Earth's mantle. Annu. Rev. Earth Planet. Sci. 36, 389–420.

Galimov, E.M., 1991. Isotope fractionation related to kimberlite magmatism and diamond formation. Geochim. Cosmochim. Acta 55, 1697–1708.

Gudmundsson, G., Wood, B.J., 1995. Experimental tests of garnet peridotite oxygen barometry. Contrib. Mineral. Petrol. 119, 56–76.

Haggerty, S.E., 1999. A diamond trilogy: superplumes, supercontinents, and supernovae. Science 285, 851–860.

Harley, S.L., 1984. An experimental study of partitioning of Fe and Mg between garnet and orthopyroxene. Contrib. Mineral. Petrol. 86, 359–373.

Jacob, D.E., Kronz, A., Viljoen, K.S., 2004. Cohenite, native iron and troilite inclusions in garnets from polycrystalline diamond aggregates. Contrib. Mineral. Petrol. 146, 566–576.

Kadik, A.A., 2006. Oxygen fugacity regime in the upper mantle as a reflection of the chemical differentiation of planetary materials. Geochem. Int. 44, 56–71.

Lazarov, M., Woodland, A.B., Brey, G.P., 2009. Thermal state and redox conditions of the Kaapvaal mantle: a study of xenoliths from the Finsch mine, South Africa. Lithos 112S, 913–923.

Luth, R.W., 1999. Carbon and carbonates in the mantle. In: Fei, Y., Bertka, C.M., Mysen, B.O. (Eds.), Mantle petrology: field observations and

high pressure experimentation: a tribute to Francis R (Joe) Boyd. The Geochemical Society, Special Publication No. 6, pp. 297–316.
Luth, R.W., Virgo, D., Boyd, F.R., Wood, B.J., 1990. Ferric iron in mantle-derived garnets. Implications for themobarometry and for the oxidation state of the mantle. Contrib. Mineral. Petrol. 104, 56–72.
Malkovets, V.G., Griffin, W.L., O'Reilly, S.Y., Wood, B.J., 2007. Diamond, subcalcic garnet, and mantle metasomatism: Kimberlite sampling patterns define the link. Geology 35, 339–342.
McCammon, C.A., Kopylova, M., 2004. A redox profile of the Slave mantle and oxygen fugacity control in the cratonic mantle. Contrib. Mineral. Petrol. 148, 55–68.
McCammon, C.A., Griffin, W.L., Shee, S.R., O'Neill, H.S.C., 2001. Oxidation during metasomatism in ultramafic xenoliths from the Wesselton kimberlite, South Africa: implications for the survival of diamond. Contrib. Mineral. Petrol. 141, 287–296.
Ohmoto, H., Kerrick, D., 1977. Devolatilization equilibria in graphitic systems. Am. J. Sci. 277, 1013–1044.
O'Neill, H.S.C., 1987. Quartz-fayalite-iron and quartz-fayalite-magnetite equilibria and the free energy formation of fayalite (Fe_2SiO_4) and magnetite (Fe_3O_4). Am. Min. 72, 67–75.
Phillips, D., Harris, J.W., Viljoen, K.S., 2004. Mineral chemistry and thermobarometry of inclusions from De Beers Pool diamonds, Kimberley, South Africa. Lithos 77, 155–179.
Pollack, H.N., Chapman, D.S., 1977. On regional variation of heat flow, geotherms, and lithospheric thickness. Tectonophysics 38, 279–296.
Rohrbach, A., Ballhaus, C., Ulmer, P., Golla-Schlindler, U., Schönbohm, D., 2011. Experimental evidence for a reduced metal-saturated upper mantle. J. Petrol. 52, 717–731.
Saxena, S.K., 1989. Oxidation state of the mantle. Geochim. Cosmochim. Acta 40, 1031–1049.
Scott, H.P., Hemley, R.J., Mao, H., Herschbach, D.R., Fried, L.E., Howard, W.M., Bastea, S., 2004. Generation of methane in the Earth's mantle. In situ high pressure-temperature measurements of carbonate reduction. Proc. Natl. Acad. Sci. U. S. A. 101, 14023–14026.
Simakov, S.K., 1998. Redox state of the Earth's upper mantle peridotites under the ancient cratons and its connection with diamond genesis. Geochim. Cosmochim. Acta 62, 1811–1820.
Sokol, A.G., Palyanova, G.A., Palyanov, Y.N., Tomilenko, A.A., Melenevsky, V.N., 2009. Fluid regime and diamond formation in the reduced mantle: experimental constraints. Geochim. Cosmochim. Acta 73, 5820–5834.
Spanu, L., Donadio, D., Hohl, D., Schwegler, E., Galli, G., 2011. Stability of hydrocarbons at deep Earth pressures and temperatures. Proc. Natl. Acad. Sci. U. S. A. 108, 6843–6846.
Stachel, T., Harris, J.W., 1997. Diamond precipitation and mantle metasomatism evidence from the trace element chemistry of silicate inclusions in diamonds from Akwatia, Ghana. Contrib. Mineral. Petrol. 129, 143–154.
Stachel, T., Harris, J.W., 2008. The origin of cratonic diamonds–constraints from mineral inclusions. Ore Geol. Rev. 34, 5–32.
Stachel, T., Harris, J.W., 2009. Formation of diamond in the Earth's mantle. J. Phys. Condens. Matter 21, 1–10.
Stagno, V., Frost, D.J., 2010. Carbon speciation in the astensphere. Experimental measurements of the redox conditions at which carbonate-bearing melts coexist with graphite or diamond in peridotite assemblages. Earth Planet. Sci. Lett. 300, 72–84.
Sunagawa, I., 1990. Growth and morphology of diamond crystals under stable and metastable conditions. J. Cryst. Growth 99, 1156–1161.
Taylor, W.R., Green, D.H., 1988. Measurements of reduced peridotite-C-O-H solidus and implications for redox melting of the mantle. Nature 332, 349–352.
Taylor, W.R., Green, D.H., 1989. The role of reduced C-O-H fluids in mantle partial melting. In: J. Ross (Ed.) Kimberlites and related rocks, Vol. 1: their composition, occurrence, origin and emplacement. Geol. Soc. Austr. Spec. Publ. 14, 592–602.
Thomassot, E., Cartigny, P., Harris, J.W., Viljoen, K.S., 2007. Methane-related diamond crystallization in the Earth's mantle: stable isotope evidences from a single diamond-bearing xenolith. Earth Planet. Sci. Lett. 257, 362–371.
Wood, B.J., Bryndzia, L.T., Johnson, K.E., 1990. Mantle oxidation state and its relationship to tectonic environment and fluid speciation. Science 248, 337–345.
Woodland, A.B., Koch, M., 2003. Variation in oxygen fugacity with depth in the upper mantle beneath the Kaapvaal craton, Southern Africa. Earth Planet. Sci. Lett. 241, 295–310.
Zhang, C., Duan, Z., 2009. A model for C-O-H fluid in the Earth's mantle. Geochim. Cosmochim. Acta 73, 2089–2102.
Zhang, C., Duan, Z., 2010. GFluid: an Excel spreadsheet for investigating C-O-H fluid composition under high temperatures and pressures. Comp. Geosc. 36, 569–572.
Ziegenbein, D., Johannes, W., 1989. Graphit-Fluid-Wechselwirkungen: Einfluß der Graphit-Kristallinität. KTB Report 90/4, 559.